SCIENTIFIC REPORTS

OPEN

SUBJECT AREAS:
ANTIBIOTICS
PEPTIDES

Received
25 June 2014

Accepted
13 October 2014

Published
31 October 2014

Correspondence and requests for materials should be addressed to J.W. (jcwu@ecust.edu.cn) or H.T. (tianhe@ecust.edu.cn)

* These authors contributed equally to this work.

# Synthesis and Antibacterial Activities of Antibacterial Peptides with a Spiropyran Fluorescence Probe

Lei Chen*, Yu Zhu*, Danling Yang, Rongfeng Zou, Junchen Wu & He Tian

Key Lab for Advanced Materials and Institute of Fine Chemicals, East China University of Science and Technology, Shanghai 200237 (P. R. China).

**In this report, antibacterial peptides1-3 were prepared with a spiropyran fluorescence probe. The probe exhibits a change in fluorescence when isomerized from a colorless spiro-form (spiropyran, Sp) to a colored open-form (merocyanine, Mc) under different chemical environments, which can be used to study the mechanism of antimicrobial activity. Peptides 1-3 exhibit a marked decrease in antimicrobial activity with increasing alkyl chain length. This is likely due to the Sp-Mc isomers in different polar environments forming different aggregate sizes in TBS, as demonstrated by time-dependent dynamic light scattering (DLS). Moreover, peptides 1-3 exhibited low cytotoxicity and hemolytic activity. These probe-modified peptides may provide a novel approach to study the effect of structural changes on antibacterial activity, thus facilitating the design of new antimicrobial agents to combat bacterial infection.**

Over the past few decades, increasing effort has been made to identify unconventional antibiotics to combat drug resistance. As a result, antimicrobial peptides (**AMPs**) have been extensively studied because of their unique mechanism of antibacterial action[1–4]. AMPs, as important components of the intrinsic defense system, display high activity and selectivity toward a wide variety of microorganisms[5–8]. However, the potential application of AMPs is hampered by several major drawbacks, such as low in vivo activity and poor bioavailability, as well as relatively high production costs[9].

Owing to these complications, a variety of synthetic antimicrobial peptides, as well as corresponding mimics, have attracted considerable interest because of their potential to overcome the shortcomings inherent in naturally occurring AMPs[10–14]. In particular, lysine-rich antimicrobial mimics displaying rapid, non-hemolytic broad-spectrum microbicidal properties have been prepared as a new class of antibacterial agents[15–16]. Although the exact mechanism of action of AMPs is not fully understood, it is commonly acknowledged that the vast majority of AMPs appear to act by permeabilizing the bacterial cell membrane, resulting in the disruption of bacterial membrane integrity and bacterial death[1–2,10]. As pioneered by Mor *et al*, it has been demonstrated that the molecular structure of AMPs has a major impact on their antibacterial activity[17]. There is still a need for the synthesis of novel antibacterial peptides in order to study their mechanism of action and thereby improve their pharmacological profile.

In recent years, molecular probes have been broadly applied in the tracking of biological species such as DNA[18–21], polysaccharides[22], cell surface proteins[23–24], enzymes[25] and even bacteria[26]. In this context, we planned to prepare photochromic-probe-modified antibacterial peptides to investigate their antibacterial activity and potential use in mechanism studies. The spiropyran compounds are excellent photochromic fluorophores and have been widely used to build functional materials[27–35] and chemical sensors[36–39] based on the photo-reversible isomerization between two thermodynamically stable states: a colorless spiro-form (spiropyran, **Sp**) and a colored open-form (merocyanine, **Mc**). Therefore, we envisioned that the introduction of a spiropyran moiety into peptides could be an efficient strategy to study the structure of antibacterial peptides by measuring the change in fluorescence based on the isomerization of spiropyran units in different polar environments[40], which further control AMP activity in time and space[41].

Herein, we designed and synthesized lysine-rich peptides **1-3** containing spiropyran moieties at both ends of the peptides linked with alkyl chains of different lengths (Figure 1). Peptides **1-3** were synthesized using a microwave-assisted solid-phase method. The antimicrobial activities of the conjugates toward Gram-positive bacteria exhibited clear differences at physiological pH. With increasing alkyl chain length, these three conjugates demonstrated different thermodynamically stable states (**Mc** and **Sp**) at physiological pH, and obviously different

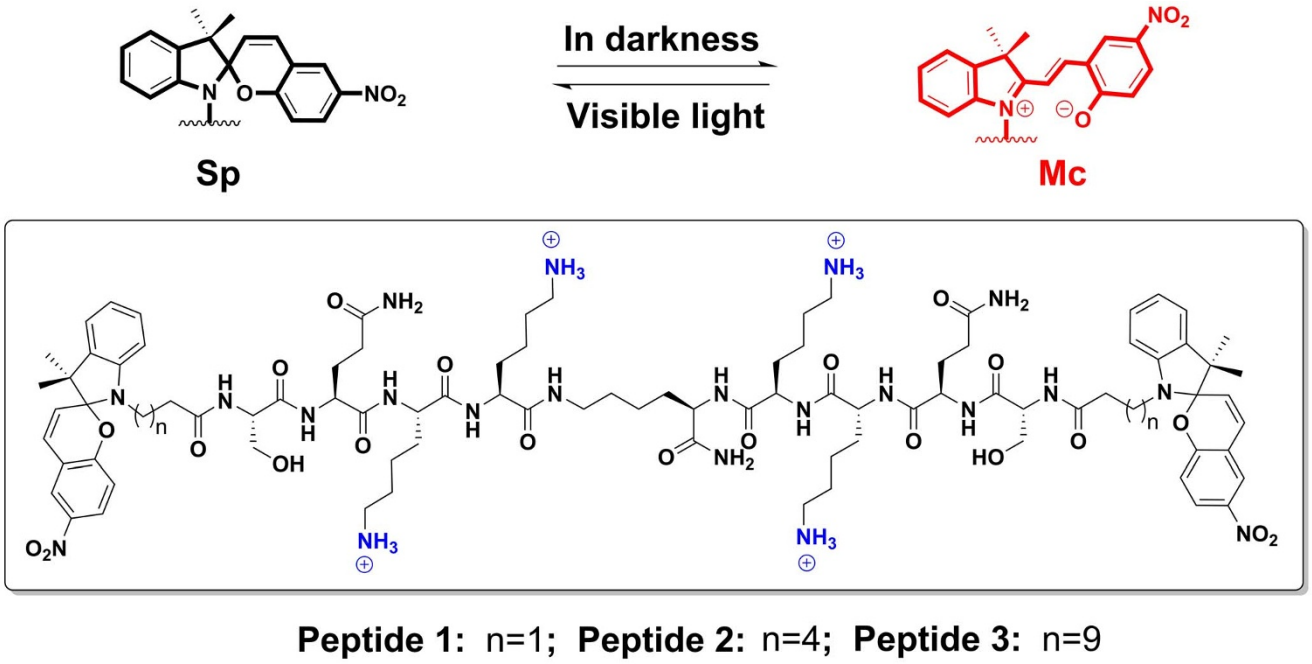


**Figure 1** | **Molecular structures of peptides 1-3.**

antimicrobial activities toward Gram-positive bacteria. Moreover, scanning electron microscopy (SEM) and confocal laser-scanning microscopy (CLSM) revealed that the bactericidal activity arose mainly through the disruption of bacterial membrane integrity, which is consistent with the common mechanism of action of antimicrobial peptides. Furthermore, the low toxicity and hemolytic activity of these peptides suggested the potential for use as antibiotics.

## Results

UV-Vis absorption and fluorescence spectra were examined in Tris-HCl buffer solutions at physiological pH[42], and the absorption changes and corresponding fluorescence emission of the probes were monitored in real time in darkness for *ca.* 8 h. At pH 7.4, peptides **1** and **2** exhibited similar optical properties, with a sharp absorption band at 514 and 508 nm, respectively (Figure 2a–2b). These maximum absorption wavelengths represented the absorption of merocyanine[43], indicating that the spiropyran units of peptides **1** and **2** were mainly in the open form of **Mc**, which is regarded as the "on" state of spiropyran. Moreover, the corresponding fluorescence peaks of peptides **1** and **2** at 620 nm were markedly increased (Figure 2d and 2e). In sharp contrast, peptide **3** did not exhibit an obvious absorption band after being placed in darkness for *ca.* 8 h (Figure 2c), suggesting a preference for the spiro-form (**Sp**), which is the "off" state. Moreover, there was no obvious change in the fluorescence of peptide **3** (Figure 2f). The different states of the peptides in the **Mc** ("On") and **Sp** ("Off") forms demonstrated changes in probe structure based on the polarity of the environment surrounding the **Sp** groups[40]. For the proximal polarity of the **Sp** groups in peptides **1**-**2** in TBS buffer, the **Mc** isomers tended to aggregate and were driven by the attractive **Mc**–**Mc** interactions. In sharp contrast, for the proximal non-polarity of the **Sp** groups in peptide **3** in TBS buffer, the process of **Mc**-**Sp** ring closing was due to an increasingly non-polar environment, in agreement with the HPLC analysis of peptides **1**-**3** (Table S1-S3 in the Supporting Information)[40]. To further confirm the state in TBS solution, the particle size distributions of peptides **1**-**3** were measured by time-dependent dynamic light scattering (DLS) at 37°C. As shown in Figure 2g–2i and Figure S1, peptides **1**-**3** formed aggregates of different sizes, with diameters as follows: peptide **1**, from 175.6 nm to 194.0 nm; peptide **2**, from 249.5 to 266.4 nm; and peptide **3**, from 267.4 to 310.6 nm. Interestingly, over the entire 8 h period in the dark, the aggregate sizes were obviously peptide **3** > peptide **2** > peptide **1**, indicating that changes in the **Mc**-**Sp** isomers could accompany changes in the polarity of the environment at 37°C in TBS (pH 7.4)[27–29,40]. Therefore, different isomers of the spiropyran units in peptides **1**-**3** could be used to indicate structural differences between peptides **1**-**3**, which may provide a new way to study the impact of structural differences on antimicrobial activity.

To determine whether antibacterial activity is affected by the aggregate sizes, we determined the antibacterial activities of peptides **1**-**3** toward typical Gram-positive and Gram-negative bacteria. The $IC_{50}$ values for each peptide (the minimum concentration that produced 50% inhibition of bacterial growth) are listed in Table 1. Interestingly, both **1** and **2** showed antibacterial activity toward Gram-positive bacteria, and **1** exhibited high bactericidal efficacy against *M. luteus* and *S. hominis*, with $IC_{50}$ values of 11.3 and 18.9 $\mu g \cdot mL^{-1}$, respectively. Peptide **2** showed preferential inhibition of *M. luteus* ($IC_{50}$ 34.0 $\mu g \cdot mL^{-1}$), with lower antibacterial activity toward Gram-positive bacteria than **1**. However, peptide **3** showed no activity against Gram-positive bacteria even at concentrations of up to 256 $\mu g \cdot mL^{-1}$. In contrast, **1** and **2** showed significant antibacterial activity at concentrations below 70.0 $\mu g \cdot mL^{-1}$.

When assayed with the same types of Gram-positive bacteria, we found that peptides **1**-**3** exhibited decreasing antibacterial activity with increasing aggregate size. As shown in Figure 3, after treatment with **1**-**2**, the growth of Gram-positive bacteria was inhibited efficiently by increasing peptide concentrations. In addition, **1** showed better antibacterial activity than **2**. However, there was no obvious inhibition for bacterial growth with treatment using **3**. As we demonstrated, the spiropyran groups in **1** and **2** are mainly in the "on" state (**Mc**), whereas in 3, the "off" state (**Sp**) was found at physiological pH. This finding indicates that the antibacterial activity of the cationic peptide can be modulated by the aggregate size. In other words, peptides showed strong antibacterial activity when they formed small aggregates in TBS, with diameters from 175.6 to 266.4 nm,

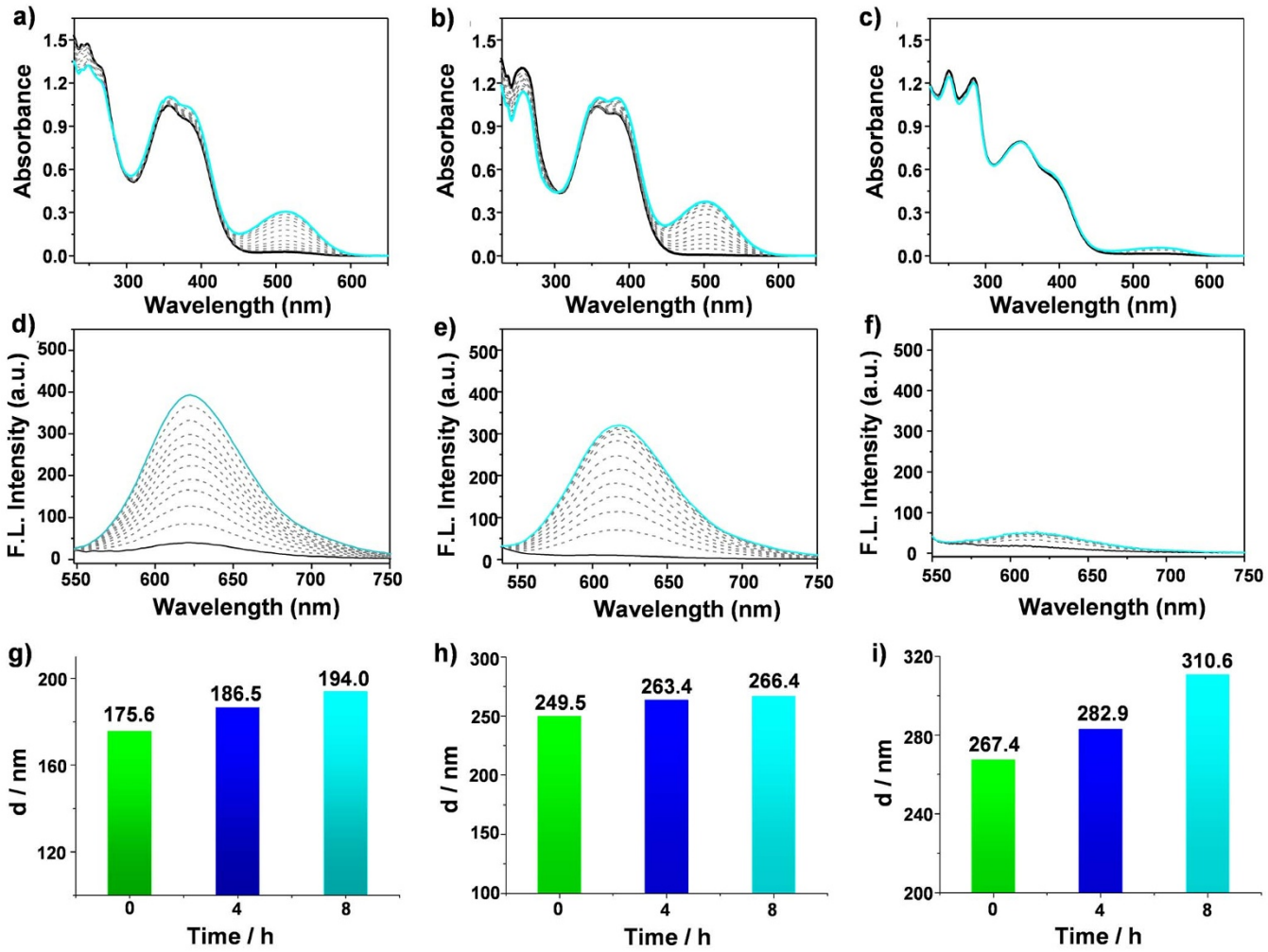


**Figure 2** | **Time-dependent absorption and fluorescence emission spectra.** Peptide **1** a) and d); **2** b) and e); **3** c) and f) (50 μM) in TBS (pH 7.4, 50 mM Tris, 50 mM NaCl, 20°C) in darkness for *ca.* 8 h. Each sample was exposed to visible light for 10 min before the assay to convert the Sp fluorophores into the closed form, and the absorption was then recorded as a function of time for *ca.* 8 h in darkness. Time-dependent DLS profiles showing distributions of hydrodynamic diameters (DH (nm)) for g) peptide **1**, h) peptide **2** and i) peptide **3** for 0 h, 4 h, and 8 h in TBS (pH 7.4, 50 mM Tris, 50 mM NaCl, 37°C).

but exhibited low activity when they formed large aggregates, with diameters from 267.4 to 310.6 nm at 37°C (Figure 2g–2i). These results, however, demonstrated that the impact of structural changes on the antibacterial activities of **1**-**3** can be directly monitored by the change in **Mc**-**Sp** isomers in different microenvironments.

In addition, the growth of Gram-positive bacteria (*M. luteus* and *S. hominis*) was efficiently inhibited by increasing concentrations of peptides **1**-**2**, whereas the growth of Gram-negative bacteria was not inhibited (Table 1 and Figure 4). Although the exact mechanism of antibacterial action remains to be understood, it seems that the bactericidal activities of AMPs are due to their ability to penetrate and disrupt the integrity of the plasma membrane[44]. Generally, Gram-positive bacteria have a simpler cell wall than Gram-negative bacteria, and the major constituent is peptidoglycan, a polysaccharide. In contrast, Gram-negative bacteria have an additional outer bilayer membrane composed of lipopolysaccharides and phospholipids[45]. Therefore, it is difficult for positively charged peptide/amphiphiles to penetrate the membrane of Gram-negative bacteria, resulting in relatively low antibacterial activity. These results were further confirmed by scanning electron microscopy (SEM) of the membrane structure (Figure 5). After treatment with peptides **1**-**3** for 12 h, the membrane structure of *M. luteus* exhibited obvious changes. The integrity of the plasma membrane was thoroughly disrupted by peptide **1** (Figure 5a), and the membrane structure collapsed after treatment with peptide **2** (Figure 5b). However, the membrane remained intact after incubation with peptide **3** (Figure 5c). Confocal laser-scanning microscopy (CLSM) was also performed to investigate the antibacterial activity of peptides **1**-**3** against *M. luteus*. We observed that peptides **1**-**2** effectively bound to *M. luteus* (Figure 5d and 5e), whereas almost no binding was observed with peptide **3** (Figure 5f). The overlay images clearly demonstrate that peptides **1**-**2** destroyed the membrane of *M. luteus*,

Table 1 | The $IC_{50}$ values of peptides 1-3 toward Gram-positive/Gram-negative bacteria

| Bacteria | Peptide 1 $IC_{50}$/μg·mL$^{-1}$ | Peptide 2 $IC_{50}$/μg·mL$^{-1}$ | Peptide 3 $IC_{50}$/μg·mL$^{-1}$ |
|---|---|---|---|
| *S. aureus* (+) [a] | 56.9 | 69.3 | >256 |
| *M. luteus* (+) | 11.3 | 34.0 | >256 |
| *S. haemolyticus* (+) | 34.1 | >128 | >256 |
| *S. hominis* (+) | 18.9 | 63.6 | >256 |
| *E. coli* (−) | 61.6 | 107.3 | >256 |
| *K. pneumoniae* (−) | >256 | >256 | >256 |
| *P. aeruginosa* (−) | >256 | >256 | >256 |
| *C. freundii* (−) | >256 | >256 | >256 |

[a] (+),(−) represent Gram-positive and Gram-negative bacteria, respectively.

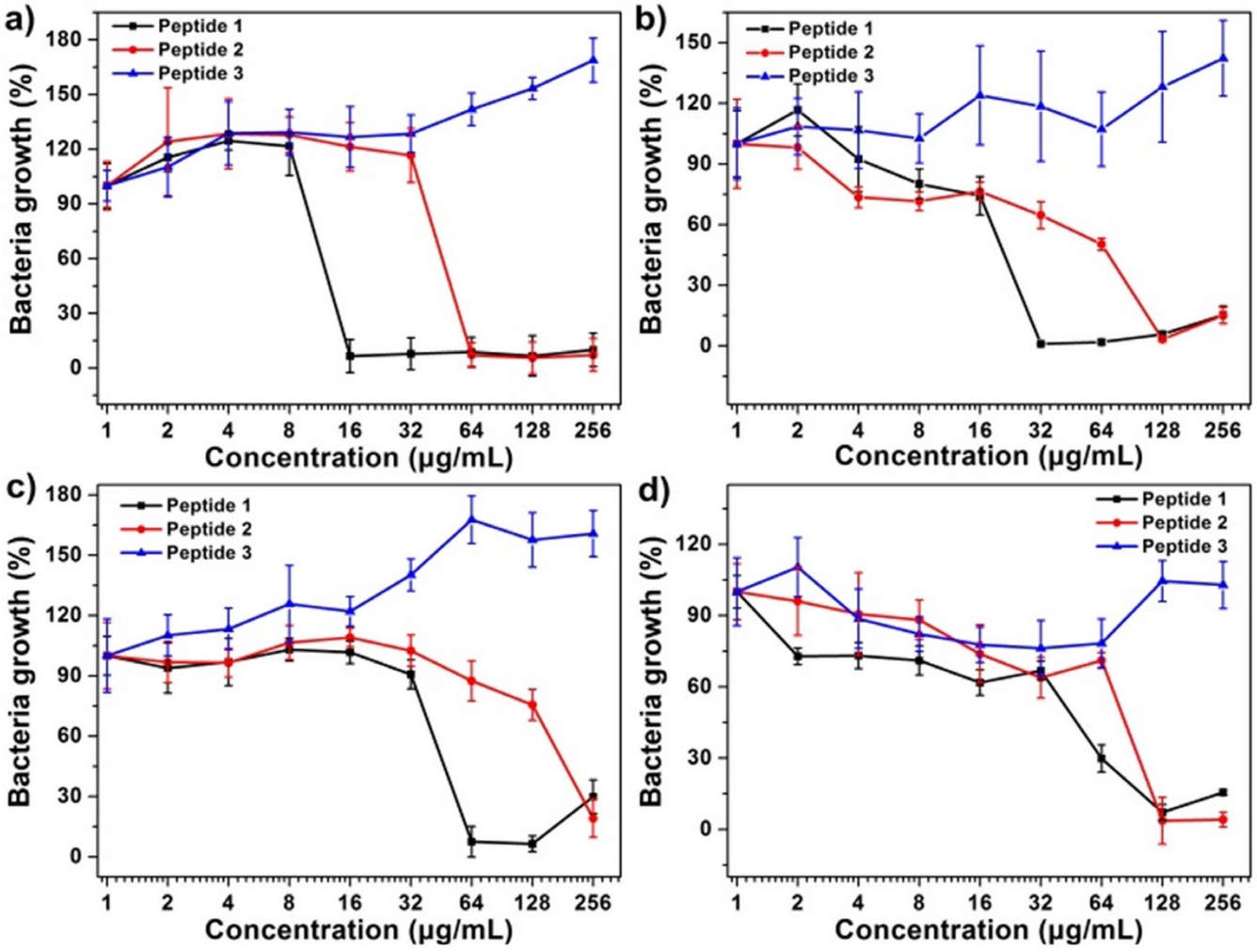


**Figure 3** | Antibacterial activities of peptides 1–3 against Gram-positive ($G^+$) bacteria: (a) *M. luteus*; (b) *S. hominis*; (c) *S. haemolyticus*; (d) *S. aureus*.

whereas peptide **3** did not (Figure 5g–5i). Thus, these results suggest that the bactericidal activity was largely due to the structural disruption of the membrane, which is in accordance with the commonly accepted mechanism of action of AMPs[46].

The antibacterial activities of peptides **1**-**3** toward Gram-positive and Gram-negative bacteria on nutrient broth medium agar plates were also investigated. As shown in Figure 6, *P. aeruginosa* grew well in nutrient broth medium, whereas the growth of *M. luteus* was

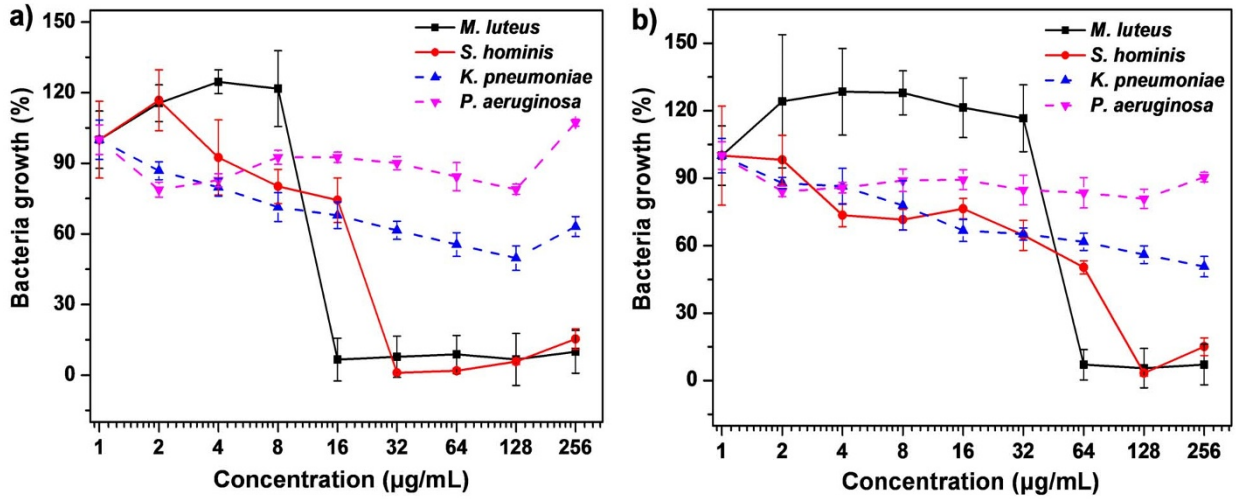


**Figure 4** | Antibacterial activity of (a) 1 and (b) 2 against Gram-positive ($G^+$) bacteria (*M. luteus*; *S. hominis*) and Gram-negative ($G^-$) bacteria (*K. pneumoniae*, *P. aeruginosa*).

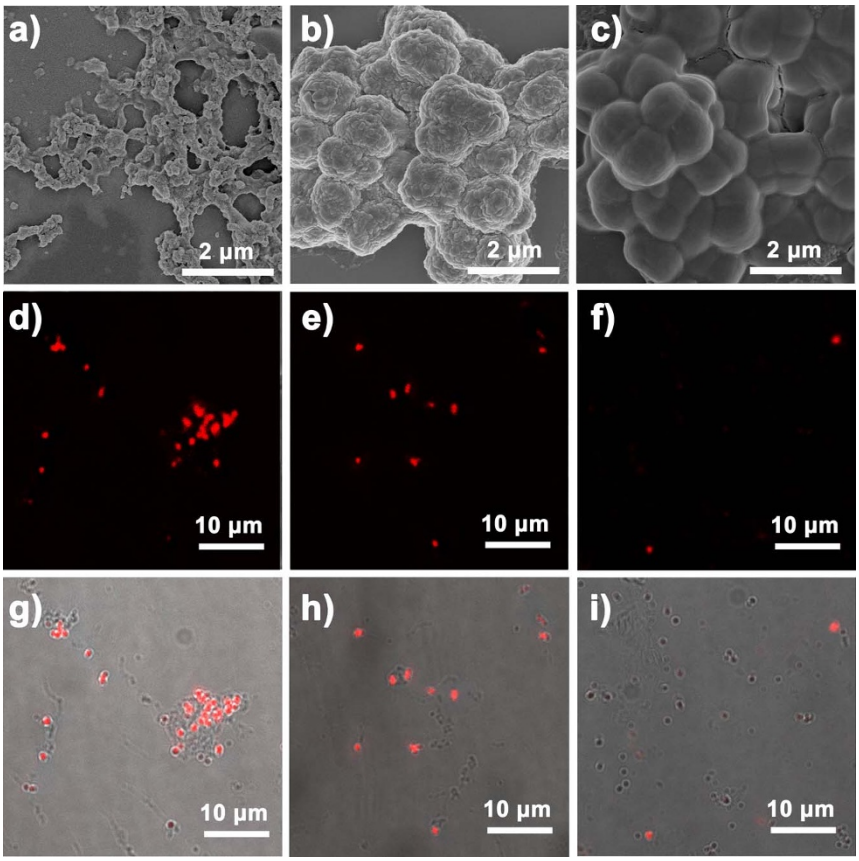


**Figure 5** | Scanning electron microscopy (SEM) images of *M. luteus*: (a–c) after treatment with peptides **1**, **2** and **3** (64 μg·mL$^{-1}$) for 12 h; confocal laser-scanning microscopy (CLSM) images of *M. luteus*: (d–f) after treatment with peptides **1**, **2** and **3** (64 μg·mL$^{-1}$) for 12 h (fluorescence field); (g–i) overlap of fluorescence and bright-field images after treatment with peptides **1**, **2** and **3** (excitation: 488 nm; emission: 570–620 nm).

efficiently inhibited by peptides **1** and **2**. Moreover, peptides **1** and **2** displayed higher antibacterial activity against *M. luteus* than did peptide **3**. These results are consistent with the $IC_{50}$ measurements.

The cytotoxicity and hemolytic activity of peptides **1**-**3** were then determined. The cellular toxicity of peptides **1**, **2** and **3** toward HeLa cells was measured by the standard 3-(4, 5-dimethyl-2-thiazolyl)-2, 5-diphenyltetrazolium bromide (MTT) assay. As shown in Figure 7a, at concentrations ranging from 0 to 40 μg·mL$^{-1}$, cell viability was estimated to remain as high as 80% after incubation for 24 h. Even at concentrations up to 60 μg·mL$^{-1}$, cell viability was still nearly 60%, suggesting low cytotoxicity of peptides **1**-**3** over a concentration range from 0 to 60 μg·mL$^{-1}$. The hemolysis test indicated that peptides 1-3 had a low hemolytic activity toward erythrocytes below the $IC_{50}$ (Figure 7b). At a concentration range from 0 to 100 μg·mL$^{-1}$, peptides **1**-**3** demonstrated a hemolytic effect at a level below 10%, and peptides **1** and **2** had lower hemolytic activity than peptide **3**. These data indicate that peptides **1**-**3** are biocompatible.

## Discussion

In summary, lysine-rich cationic peptides **1**-**3**, containing a spiropyran moiety linked to alkyl chains of different lengths were synthesized, and their antibacterial activities were studied by monitoring structural isomerization of the spiropyran group in different microenvironments. We demonstrated that probes **1**-**3** can be used to

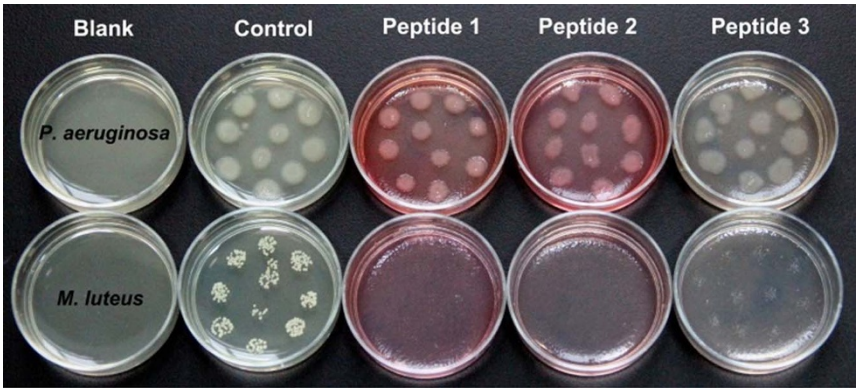


**Figure 6** | **Antibacterial activity of peptides 1-3 toward *P. aeruginosa* (G$^-$) and *M. luteus* (G$^+$) on nutrient broth medium agar.**

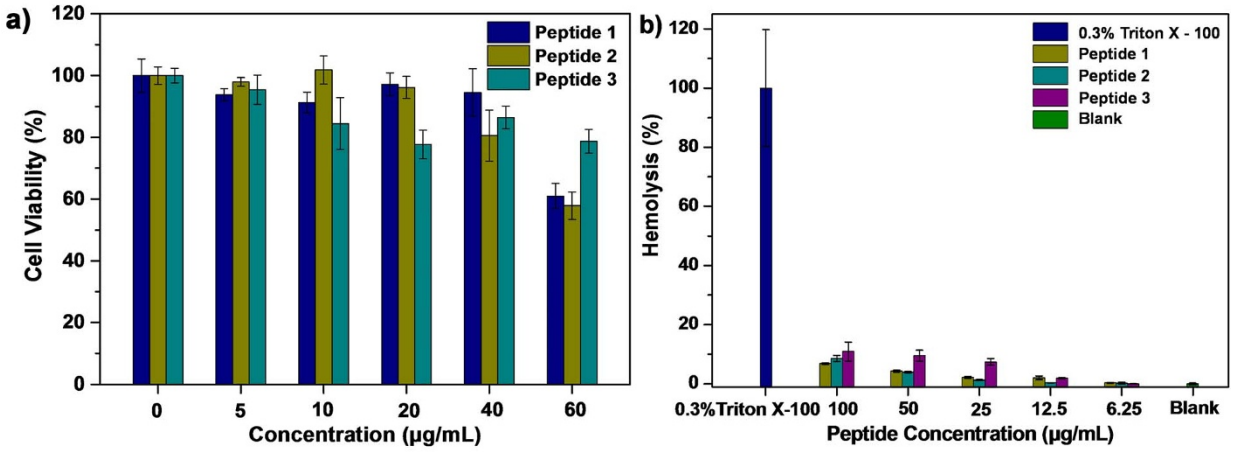


**Figure 7** | (a) Cell viability (%) of HeLa cells after incubation with different concentrations of peptides 1, 2 and 3 for 24 h; (b) Hemolytic activity of peptides **1**, **2** and **3** at different concentrations.

monitor the change in **Mc-Sp** isomers at physiological pH from time-dependent absorption and fluorescence emission spectra. In addition, the aggregation states of probes **1-3** were investigated by time-dependent DLS, and the results showed that **1-3** formed different-sized aggregates (peptide **3** > peptide **2** > peptide **1**), leading to decreased antibacterial activity. Furthermore, the low cytotoxicity and hemolytic effects of peptides **1-3** indicate good biocompatibility. These probe-modified peptides may provide an opportunity to study the effects of structural changes on antibacterial activity, aiding in the design of new antimicrobial agents to combat bacterial infections.

## Methods

**UV-Vis absorption study.** The UV-Vis and fluorescence spectra were recorded at 20°C on a Varian Cary 100 Conc UV-Visible Spectrometer and a Varian Cary Eclipse Fluorescence Spectrometer, respectively. The samples were excited at the wavelength appropriate for the fluorescent peptides. The slit widths were set to 10 nm for excitation and emission. The data points were collected at 1-nm increments with a 0.1 s integration period. All spectra were corrected for intensity using the manufacturer-supplied correction factors and corrected for background fluorescence and absorption by subtracting a blank scan of the buffer system. The UV-Vis absorption and fluorescence spectroscopy were studied in Tris-HCl buffer solutions (TBS) at pH 7.4. Each sample was treated with visible light for 10 min prior to measuring to ensure the SP fluorophores were in the closed-form, and corresponding absorption and fluorescence emission measurements were then recorded as a function of time for 8 h in darkness without UV light.

**Time-dependent dynamic light scattering (DLS) assay.** All DLS experiments were performed on a Malvern Instruments Zetasizer Nano ZS at 37°C, and the starting solutions were filtered prior to use. Samples of peptides 1-3 were prepared in TBS (pH 7.4, 50 mM Tris, 50 mM NaCl) in a total sample volume of 1.0 mL. Each sample was exposed to visible light for 10 min before measurement to ensure the SP fluorophores were in the closed form, and the corresponding DLS measurements were then recorded as a function of time for 0 h, 4 h, and 8 h in darkness without UV-Vis light.

**Antibacterial activity assay.** All bacteria were obtained from the College of Public Health of Nantong University, China. Four Gram-positive bacteria (*Staphylococcus aureus* ATCC-25923, *Micrococcus luteus* ATCC–4698, *Staphylococcus hominis* ATCC-27844, and *Staphylococcus haemolyticus*, ATCC–29970) and four Gram-negative bacteria (*Escherichia coli* ATCC-25922, *Klebsiella pneumoniae* ATCC-700603, *Pseudomonas aeruginosa* ATCC-27853, and *Citrobacter freundii* ATCC-13316) were used in this assay. A representative colony was lifted off with a wire loop and placed in 5 mL of nutrient broth medium, which was then incubated with shaking at 37°C for 5 h. Then, $1 \times 10^6$ cells/mL were suspended in nutrient broth medium to generate the working suspension. Different concentrations of peptides were prepared in a 96-well plate using nutrient broth medium, and each well contained 100 μL compound solutions. A 100-μL cell working suspension was then added to each well. The plate was incubated at 37°C for 24 h, and the optical density (OD) of each well was then measured at 600 nm after gently shaking the plate for 10 s using a Hybrid Multi-Mode Microplate reader (BioTek, Synergy H4). Wells containing medium only (blank) and wells containing cells in medium without peptides (positive control) were included on the same plate. The percentage of cell growth in each well was calculated as follows: Bacteria Growth (%) = [(AP – AB)/(AC – AB)] × 100), where AP is the mean absorbance value for a known peptide concentration, AC is the mean absorbance value for the positive control and AB is the mean absorbance value for blank. The resultant values were then plotted as a function of the peptide concentration to generate dose-response curves of antibacterial activity for each peptide. The $IC_{50}$ is the minimum concentration that produces 50% inhibition of bacterial growth.

**Scanning electron microscopy (SEM).** Bacterial cells (*Micrococcus luteus*) were inoculated and cultured in nutrient broth medium with shaking at 37°C for approximately 5 h and suspended in nutrient broth medium at a density of $1 \times 10^6$ cells/mL for use. Then, peptides **1-3** were incubated with bacteria at 37°C for 12 h in nutrient broth medium at a concentration of 64 μg/mL; the control group contained bacteria only. After incubation, the samples were centrifuged at 7,500 rpm for 5 min, and the supernatant was removed. The bacteria were washed three times with PBS, suspended in pure water, placed (10 μL) onto the mica plate, and dried at room temperature. The SEM images were recorded with NOVA Nano SEM 450 equipment.

**Confocal laser-scanning microscopy (CLSM).** Bacterial cells (*M. luteus*) were inoculated and cultured in nutrient broth medium with shaking at 37°C for 5 h and suspended in nutrient broth medium at a density of $1 \times 10^6$ cells/mL for use. Then, peptides **1-3** were incubated with bacteria at 37°C for 12 h in nutrient broth medium at a concentration of 64 μg/mL; the control group contained bacteria only. After incubation, the cells were centrifuged at 7,500 rpm for 7 min, and the supernatant was removed. The bacteria were washed three times with PBS, suspended in pure water, placed (2 μL) onto the microscope slide, and dried at room temperature. CLSM images were obtained using a Nikon AIR confocal laser-scanning microscope equipped with a 100x oil-immersion objective lens. Excitation was performed at 488 nm, and emission was measured at 570–620 nm.

**Antibacterial activity assay on nutrient broth medium agar plate.** Nutrient broth medium agar was sterilized at 121°C for 15 min and kept at 45–50°C in a thermostat water bath before use. Bacterial cells (*Micrococcus luteus* and *Pseudomonas aeruginosa*) were inoculated and cultured in nutrient broth medium with shaking at 37°C for approximately 5 h and suspended in nutrient broth medium at $1 \times 10^6$ cells/mL. The peptides were added to the sterilized nutrient broth medium agar at a final concentration of 64 μg/mL and 128 μg/mL. *Micrococcus luteus* and *Pseudomonas aeruginosa* were added onto the peptide-containing agar plates and cultured for 24 h at 37°C.

**Cytotoxicity assay.** All cell lines were purchased from Shanghai Bogoo Biotech Co., Ltd., China. Cytotoxicity was measured using the 3-(4, 5-dimethylthiazol-2-yl)-2, 5-diphenyltetrazolium bromide (MTT) assay in HeLa cells. Cells growing in log phase were seeded onto a 96-well cell-culture plate at $1 \times 10^5$/well. The cells were incubated for 24 h at 37°C under 5% $CO_2$. A solution of peptides **1-3** (100.0 μL/well) at concentrations of 2, 4, 8, 16, 32, 64 μg/mL in DMEM was added to the wells of the treatment group, whereas for the negative control group, 100.0 μL of DMEM alone was added. The cells were incubated for 24 h at 37°C under 5% $CO_2$. After removal of the medium, a solution of 0.5 mg/mL MTT (100 μL/well) was added to the plates for an additional 4 h of incubation, allowing viable cells to reduce the yellow tetrazolium salt (MTT) into dark-blue formazan crystals. After removal of the medium, formazan extraction was performed with 100 μL DMSO, and the amount of formazan was determined colorimetrically using a plate reader (BioTek, Synergy H4), which was used to measure the OD 490 nm (Absorbance value). The following formula was used to calculate cell viability: Viability (%) = (mean Absorbance value of treatment group/mean Absorbance value of control) × 100.

**Hemolysis assay.** Fresh human blood (1 mL) was provided by a healthy donor (age 45, Female) from a clinical laboratory at an affiliated hospital of Nantong University,

China. This protocol was approved by the ethics committee of the affiliated hospital of Nantong University in accordance with the guidelines for the care and use of laboratory clinical blood samples. Centrifugation was carried out at 3,700 rpm for 5 min to separate the erythrocytes. The separated erythrocytes were washed thrice with TBS (10 mM Tris, 150 mM NaCl, pH 7.2) before dilution to a final concentration of 2% (v/v). The erythrocyte suspension (200 μL) was added to the peptides (200 μL) ranging in concentration from 6.25 to 100 μg/mL in centrifuge tubes and incubated at 37°C for 1 h. After incubation, the tubes were centrifuged at 3,700 rpm for 5 min, and the supernatant (100 μL) was added to the wells of a 96-well microplate. The absorbance of the solution at 540 nm was read on a Microplate reader. The positive control consisted of 0.1% Triton X-100, and Tris buffer served as the negative control. The following formula was used to calculate the percentage of hemolysis: Hemolysis (%) = $[(A_P - A_B)/(A_C - A_B)] \times 100$, where $A_P$ is the absorbance value for a known peptide concentration, $A_C$ is the absorbance value for the Triton X-100 positive control and $A_B$ is the absorbance value for Tris buffer.


1. Toke, O. Antimicrobial peptides: New candidates in the fight against bacterial infections. *Biopolymers* **80**, 717–735 (2005).
2. Nguyen, L. T., Haney, E. F. & Vogel, H. J. The expanding scope of antimicrobial peptide structures and their modes of action. *Trends Biotechnol.* **29**, 464–472 (2011).
3. Andreu, D., Rivas, L. & others. Animal antimicrobial peptides: an overview. *Biopolymers* **47**, 415–433 (1998).
4. Chatterjee, C., Paul, M., Xie, L. & van der Donk, W. A. Biosynthesis and mode of action of lantibiotics. *Chem. Rev.* **105**, 633–684 (2005).
5. Tossi, A., Sandri, L. & Giangaspero, A. Amphipathic, α-helical antimicrobial peptides. *Biopolymers* **55**, 4–30 (2000).
6. Ganz, T. Defensins: antimicrobial peptides of innate immunity. *Nat. Rev. Immunol.* **3**, 710–720 (2003).
7. Finlay, B. B. & Hancock, R. E. W. Can innate immunity be enhanced to treat microbial infections? *Nat. Rev. Micro.* **2**, 497–504 (2004).
8. Van't Hof, W., Veerman, E. C., Helmerhorst, E. J. & Amerongen, A. V. Antimicrobial peptides: properties and applicability. *Biol. Chem.* **382**, 597–619 (2001).
9. Latham, P. W. Therapeutic peptides revisited. *Nat. Biotechnol.* **17**, 755–758 (1999).
10. Som, A., Vemparala, S., Ivanov, I. & Tew, G. N. Synthetic mimics of antimicrobial peptides. *Biopolymers* **90**, 83–93 (2008).
11. Debnath, S., Shome, A., Das, D. & Das, P. K. Hydrogelation through self-assembly of Fmoc-peptide functionalized cationic amphiphiles: potent antibacterial agent. *J. Phys. Chem. B* **114**, 4407–4415 (2010).
12. Fernandez-Lopez, S. *et al*. Antibacterial agents based on the cyclic d,l-α-peptide architecture. *Nature* **412**, 452–455 (2001).
13. Li, P. *et al*. A polycationic antimicrobial and biocompatible hydrogel with microbe membrane suctioning ability. *Nat. Mater.* **10**, 149–156 (2011).
14. Salick, D. A., Kretsinger, J. K., Pochan, D. J. & Schneider, J. P. Inherent antibacterial activity of a peptide-based β-Hairpin hydrogel. *J. Am. Chem. Soc.* **129**, 14793–14799 (2007).
15. Radzishevsky, I., Krugliak, M., Ginsburg, H. & Mor, A. Antiplasmodial activity of lauryl-lysine oligomers. *Antimicrob. Agents Chemother.* **51**, 1753–1759 (2007).
16. Radzishevsky, I. S. *et al*. Structure-activity relationships of antibacterial acyl-lysine oligomers. *Chem. Biol.* **15**, 354–362 (2008).
17. Sarig, H., Rotem, S., Ziserman, L., Danino, D. & Mor, A. Impact of self-assembly properties on antibacterial activity of short acyl-lysine oligomers. *Antimicrob. Agents Chemother.* **52**, 4308–4314 (2008).
18. Liang, H. *et al*. Functional DNA-containing nanomaterials: cellular applications in biosensing, imaging, and targeted therapy. *Acc. Chem. Res.* **47**, 1891–1901 (2014).
19. Lu, C.-H., Cecconello, A., Elbaz, J., Credi, A. & Willner, I. A three-station DNA catenane rotary motor with controlled directionality. *Nano Lett.* **13**, 2303–2308 (2013).
20. Wu, J. *et al*. A molecular peptide beacon for the ratiometric sensing of nucleic acids. *J. Am. Chem. Soc.* **134**, 1958–1961 (2012).
21. Zhang, P., Beck, T. & Tan, W. Design of a molecular beacon DNA probe with two fluorophores. *Angew. Chem.* **113**, 416–419 (2001).
22. Huang, Y.-J. *et al*. Glucose sensing via aggregation and the use of 'Knock-Out' binding to improve selectivity. *J. Am. Chem. Soc.* **135**, 1700–1703 (2013).
23. Shi, H. *et al*. Activatable aptamer probe for contrast-enhanced in vivo cancer imaging based on cell membrane protein-triggered conformation alteration. *Proc. Natl. Acad. Sci. U. S. A.* **108**, 3900–3905 (2011).
24. Yang, C. J., Jockusch, S., Vicens, M., Turro, N. J. & Tan, W. Light-switching excimer probes for rapid protein monitoring in complex biological fluids. *Proc. Natl. Acad. Sci. U. S. A. of the United States of America* **102**, 17278–17283 (2005).
25. Wang, Q. *et al*. A fluorescent light-up probe as an inhibitor of intracellular β-tryptase. *Chem. Commun.* **50**, 6120–6122 (2014).
26. Leevy, W. M. *et al*. Optical Imaging of bacterial infection in living mice using a fluorescent near-infrared molecular probe. *J. Am. Chem. Soc.* **128**, 16476–16477 (2006).
27. Sheng, L. *et al*. Hydrochromic molecular switches for water-jet rewritable paper. *Nat. Commun.* **5**, 3044 (2014).
28. Wang, F., Liu, X. & Willner, I. Integration of photoswitchable proteins, photosynthetic reaction centers and semiconductor/biomolecule hybrids with electrode supports for optobioelectronic applications. *Adv. Mater.* **25**, 349–377 (2013).
29. Setaro, A., Bluemmel, P., Maity, C., Hecht, S. & Reich, S. Non-covalent functionalization of individual nanotubes with spiropyran-based molecular switches. *Adv. Funct. Mater.* **22**, 2425–2431 (2012).
30. Kawata, S. & Kawata, Y. Three-dimensional optical data storage using photochromic materials. *Chem. Rev.* **100**, 1777–1788 (2000).
31. Berkovic, G., Krongauz, V. & Weiss, V. Spiropyrans and spirooxazines for memories and switches. *Chem. Rev.* **100**, 1741–1754 (2000).
32. Balzani, V., Credi, A. & Venturi, M. Molecular logic circuits. *ChemPhysChem* **4**, 49–59 (2003).
33. Balzani, V., Credi, A. & Venturi, M. Light powered molecular machines. *Chem. Soc. Rev.* **38**, 1542–1550 (2009).
34. Hammarson, M., Nilsson, J. R., Li, S., Beke-Somfai, T. & Andréasson, J. Characterization of the thermal and photoinduced reactions of photochromic spiropyrans in aqueous solution. *J. Phys. Chem. B* **117**, 13561–13571 (2013).
35. Nilsson, J. R. *et al*. Switching properties of a spiropyran–cucurbit[7]uril supramolecular assembly: usefulness of the anchor approach. *ChemPhysChem* **13**, 3691–3699 (2012).
36. Shao, N. *et al*. A Spiropyran-based ensemble for visual recognition and quantification of cysteine and homocysteine at physiological levels. *Angew. Chem.* **118**, 5066–5070 (2006).
37. Andersson, J., Li, S., Lincoln, P. & Andréasson, J. Photoswitched DNA-binding of a photochromic spiropyran. *J. Am. Chem. Soc.* **130**, 11836–11837 (2008).
38. Xie, X., Mistlberger, G. & Bakker, E. Reversible photodynamic chloride-selective sensor based on photochromic spiropyran. *J. Am. Chem. Soc.* **134**, 16929–16932 (2012).
39. Jonsson, F., Beke-Somfai, T., Andréasson, J. & Nordén, B. Interactions of a photochromic spiropyran with liposome model membranes. *Langmuir* **29**, 2099–2103 (2013).
40. Klajn, R. Spiropyran-based dynamic materials. *Chem. Soc. Rev.* **43**, 148 (2014).
41. Velema, W. A., Szymanski, W. & Feringa, B. L. Photopharmacology: Beyond Proof of Principle. *J. Am. Chem. Soc.* **136**, 2178–2191 (2014).
42. Chen, L., Wu, J., Schmuck, C. & Tian, H. A switchable peptide sensor for real-time lysosomal tracking. *Chem. Commun.* **50**, 6443 (2014).
43. Satoh, T., Sumaru, K., Takagi, T., Takai, K. & Kanamori, T. Isomerization of spirobenzopyrans bearing electron-donating and electron-withdrawing groups in acidic aqueous solutions. *Phys. Chem. Chem. Phys.* **13**, 7322 (2011).
44. Harriman, A. (Photo) isomerization dynamics of merocyanine dyes in solution. *J. Photochem. Photobiol., A* **65**, 79–93 (1992).
45. Shai, Y. Mode of action of membrane active antimicrobial peptides. *Biopolymers* **66**, 236–248 (2002).
46. Haldar, J., Kondaiah, P. & Bhattacharya, S. Synthesis and antibacterial properties of novel hydrolyzable cationic amphiphiles. Incorporation of multiple head groups leads to impressive antibacterial activity. *J. Med. Chem.* **48**, 3823–3831 (2005).


## Acknowledgments

We thank the National Basic Research 973 Program (2013CB733700), the Fundamental Research Funds for the Central Universities (WJ1213007) and the Innovation Program of Shanghai Municipal Education Commission (J100-2-13104) for financial support.

## Author contributions

L. C., Y. Z., D. L. Y. and R. F. Z. performed the experiments and analyzed the data; J. C. W. designed the experiments and supervised the project; and J. C. W. and H. T. wrote the paper.

## Additional information

**Supplementary information** accompanies this paper at http://www.nature.com/scientificreports

**Competing financial interests:** The authors declare no competing financial interests.

**How to cite this article:** Chen, L. *et al*. Synthesis and Antibacterial Activities of Antibacterial Peptides with a Spiropyran Fluorescence Probe. *Sci. Rep.* **4**, 6860; DOI:10.1038/srep06860 (2014).